J. T. K. L.
JURNAL TEKNIK KIMIA DAN LINGKUNGAN

Adsorption Kinetics and Process Parameter Effects on Oil Uptake by Tamarind Fruit-Shell Activated Carbon

Lusi Ernawati[1,*], Eka Masrifatus Anifah[2], Musyarofah[3], Mutia Reza[1], Joko Waluyo[4], Norzahir Sapawe[5]

[1]Department of Chemical Engineering, Institut Teknologi Kalimantan, Jl. Soekarno Hatta KM 15, Balikpapan, Kalimantan Timur, 76127, Indonesia
[2]Department of Environmental Engineering, Institut Teknologi Kalimantan, Jl. Soekarno Hatta KM 15, Balikpapan, Kalimantan Timur, 76127, Indonesia
[3]Department of Physics, Institut Teknologi Kalimantan, Jl. Soekarno Hatta KM 15, Balikpapan, Kalimantan Timur, 76127, Indonesia
[4]Department of Chemical Engineering, Faculty of Engineering, Universitas Sebelas Maret, Jl. Ir. Sutami No. 36A, Kentingan, Surakarta, 57126, Indonesia
[5]Universiti Kuala Lumpur Branch Campus Malaysian Institute of Chemical and Bioengineering Technology (UniKL MICET), Lot 1988 Vendor City, Taboh Naning, 78000 Alor Gajah, Melaka, Malaysia

ABSTRACT

Oil contamination presents a major challenge to wastewater treatment systems due to its detrimental effects. This research explores the effectiveness of activated carbon derived from tamarind fruit shells as an adsorbent for removing oil from wastewater. The activated carbon was prepared using three different chemical agents: phosphoric acid, zinc chloride, and sodium hydroxide. Characterization of the resulting carbon materials was performed using XRD, FTIR, SEM, and BET analysis. Batch adsorption experiments were conducted to evaluate the influence of initial oil concentration, adsorbent dosage, contact time, temperature, and pH. The BET specific surface area, pore size and total pore volume for the optimum adsorption capacity of activated carbon using H_3PO_4 are obtained at 617.59 $m^2.g^{-1}$, 37.14 $cm^3.g^{-1}$ and 0.812 $g.g^{-1}$, respectively. Optimal adsorption occurred at an oil concentration of 5000 $mg.L^{-1}$, a dosage of 1 $g.L^{-1}$, a contact time of 60 minutes, a temperature of 60°C, and neutral pH (7). Across all activating agents, the Langmuir isotherm best described the adsorption equilibrium, while adsorption kinetics followed the pseudo-second-order model. Among the samples, activated carbon treated with H_3PO_4 demonstrated the highest adsorption capacity (1070 $mg.g^{-1}$), followed by $ZnCl_2$ (879 $mg.g^{-1}$), and NaOH (643 $mg.g^{-1}$). These results indicate that tamarind shell-derived activated carbon is a cost-effective and efficient solution for oil removal in wastewater treatment applications.

Keywords: activated-carbon, adsorption, chemical activation, isotherm, lubricant oil, tamarind shell.

1. INTRODUCTION

Southeast Asia has become a major force in the global automotive industry, accounting for the largest share of the region's overall manufacturing output [1,2]. Indonesia is one of the country in Southeast Asia holds the largest market share in automotive sector, with annual vehicle production reaching approximately 2 million units [3]. The rapid growth in automobile manufacturing and ownership has led to a notable increase in the number of automotive repair facilities. These repair services typically involve routine maintenance operations such as engine repairs and oil changes. Such activities frequently produce various types of waste, including used lubricants, wastewater, hazardous solid waste, and exhaust emissions [4]. Among these, oil and heavy metals is common byproducts of automotive maintenance pose a significant risk of contamination to soil and water resources [5]. Automotive repair activities generate various pollutants including spent lubricants, heavy hydrocarbons (such as tar, grease, and diesel), emulsified oils, suspended solids, and

heavy metals [6] which can contaminate water sources and contribute to the formation of oily wastewater. The release of such wastewater into the environment poses a serious threat to aquatic ecosystems. When oil forms a surface layer on water bodies, it obstructs oxygen transfer from the atmosphere, resulting in reduced dissolved oxygen levels [7]. Additionally, polyaromatic hydrocarbons (PAHs) commonly found in oily wastewater can inhibit plant growth and are known to have carcinogenic properties [8]. Various methods are available for removing oil contaminants from oily wastewater, including biological treatment [9], membrane separation [10], coagulation-flocculation [11], and adsorption [12]. Among these, biological treatment is environmentally sustainable but requires long retention times and is challenged by the toxicity of hydrocarbons to microorganisms. While membrane technologies offer high removal efficiency, they are often cost-prohibitive. Chemical process such as coagulation-flocculation methods, though effective, generate chemical sludge that can pose environmental hazards. Adsorption stands out as a highly efficient and widely used technique, primarily due to the exceptional surface area and porosity of activated carbon, which enhances its capacity to trap oil. To reduce costs, researchers have explored the production of activated carbon from agricultural biomass waste as an alternative to commercial variants. Agricultural waste-derived adsorbents are favored for being abundant, eco-friendly, and locally accessible. Previous studies have demonstrated the potential of such materials including eggplant [13], eucalyptus bark [14], banana peels [15], and corn stalks [16] in effectively adsorbing oil from oily wastewater. In this context, activated carbon has been widely recognized as a highly effective adsorbent for oil removal from aqueous environments.

The effectiveness of activated carbon is primarily attributed to its exceptionally high surface area, extensive porosity, and strong chemical affinity for organic compounds, including hydrocarbons. These properties enable it to adsorb large quantities of oil by providing abundant active sites for interaction and retention. The microporous and mesoporous structures of activated carbon facilitate the diffusion of oil molecules into its internal pores, thereby enhancing adsorption capacity. Additionally, its surface chemistry can be tailored through physical or chemical activation processes to improve selectivity and performance in specific applications.

Despite its widespread use, the performance of activated carbon can vary significantly depending on its source material and activation method. This study explores the preparation and characterization of activated carbon derived from tamarind fruit shells, with the aim of optimizing its structure and surface properties for efficient oil adsorption. Tamarind is a tropical plant native to South and Southeast Asia, widely cultivated for its fruit, which is commonly used in food and pharmaceutical industries. After processing the fruit, the tamarind shells are typically discarded as waste. However, due to their abundance and low cost, these fruit shells offer promising potential as adsorbents for wastewater treatment. Prior studies have demonstrated that chemically activated tamarind shells are effective in adsorbing heavy metals [17,18], dyes [19], and fluoride [20] from aqueous solutions. Chemical activation, using either acids or bases, enhances the adsorption characteristics of carbon materials. For instance, phosphoric acid (H_3PO_4) improves adsorptive efficiency [21], while sodium hydroxide (NaOH) and zinc chloride ($ZnCl_2$) enhance surface area and microporosity, thereby boosting adsorption performance [22].

Despite several studies on adsorption using chemically activated tamarind shells, there is a notable lack of research on their application for oil removal from oily wastewater and the influence of different activating agents. This study, therefore, aims to evaluate the effectiveness of tamarind shell-derived activated carbon in oil adsorption and to investigate how various chemical activation

agents impact its performance. By understanding the relationship between activation parameters and adsorption efficiency, this research contributes to the development of sustainable and high-performance adsorbents for oil spill remediation and wastewater treatment.

2. RESEARCH METHODS
2.1. Adsorbent Preparation
Tamarind fruit shells were sourced from agricultural land in North Penajam. The shells were thoroughly washed and ground into powder form. To remove impurities, the powdered material was soaked in a 0.5 M hydrochloric acid (HCl, Supelco, 37%) solution for 3 hours. After acid treatment, the sample was rinsed with demineralized water and oven-dried at 110°C for 3 hours to eliminate moisture. Carbonization was carried out at 500°C for 4 hours in a furnace, after which the resulting carbon was sieved to obtain particles of 60 mesh size. The tamarind-derived carbon was then subjected to chemical activation using phosphoric acid (H_3PO_4, Sigma-Aldrich, 99.99%), zinc chloride ($ZnCl_2$, Supelco, 98%), and sodium hydroxide (NaOH, Supelco, 99.99%). For activation, 10 grams of carbon were immersed in each activating solution at a 1:20 weight-to-volume (w/v) ratio for 24 hours. After activation, the carbon was washed with demineralized water until a neutral pH was achieved, then dried again at 110°C for 3 hours to obtain the final activated adsorbent.

2.2. Adsorbent Characterization
A series of characterization techniques were conducted to evaluate the properties of the prepared samples. Surface morphology was examined using scanning electron microscopy (SEM, Thermoscientific, Type phenom pro-X) at an accelerating voltage of 15 kV. To identify chemical bonds, Fourier-transform infrared spectroscopy (FTIR, Perkin Elmer Spectrum BX) was performed using KBr pellet samples, scanning in the range of 400 to 4,000 cm^{-1}. The crystalline structure was determined via powder X-ray diffraction (XRD) using a PAN-analytical X'Pert Pro-diffractometer with Cu-Kα radiation (40 kV, 40 mA) and a 2θ scanning range from 10° to 100° at a resolution of 0.05°. Lastly, the specific surface area (SSA) was assessed using Brunauer–Emmett–Teller (BET) analysis (NOVA 4200-E), based on N_2 adsorption/desorption isotherms at 77 K, after pre-drying the samples at 200 °C in a nitrogen atmosphere for 3 hours.

2.3. Adsorption Studies
Batch adsorption experiments were performed using synthetic oily wastewater prepared by adding used lubricant oil collected from automotive repair stations into demineralized water. Each experiment was conducted in a 250 mL volume of the synthetic oily wastewater. Key operational variables included an initial oil concentration ranging from 5000 to 15,000 mg.L^{-1}, contact times from 0 to 60 minutes, adsorbent dosages between 0.5 and 1.5 grams, temperatures ranging from 30°C to 70°C, and pH levels between 4 and 7. The effect of the initial oil concentration experiment was investigated using a dose of 1 gram per 250 mL with a contact time of 60 minutes. A batch experiment under different contact times was carried out to determine the equilibrium time of oil adsorption. During the batch experiment, the dose of 1 gram per 250 mL, with an initial concentration of 5000 mg. L^{-1}, was kept constant. The effect of dose studies was conducted using a 250 mL solution with 5000 mg of an initial oil concentration, mixed at a rate of 800 rpm for 60 minutes. The dose of 1 gram per 250 ml, initial oil concentration of 5000 mg.L^{-1}, and contact time of 30 minutes were used to investigate the effect of temperature on oil adsorption. The effect of pH experiments was carried out in a dose of 1 gram per 250 mL, with an initial concentration of 5000 mg.L^{-1}, and a contact time of 1 hour. The activated carbon adsorbent was introduced into the solution and agitated using a magnetic stirrer at 800 rpm to ensure uniform mixing. Following the adsorption process, the mixture was centrifuged at 2500 rpm for 15 minutes to separate the solid adsorbent from

the solution. The resulting precipitate was then dried in an oven at 110°C for 1 hour. Oil adsorption capacity was quantified through gravimetric analysis. The adsorbed oil onto adsorbents was calculated using equation (1), and the oil adsorption capacity was determined using equation (2).

$$\text{Oil removal efficiency (\%)} = \frac{m_f}{m_o} \times 100\% \quad (1)$$

$$\text{Oil adsorption capacity} \left(\frac{g}{g}\right) = \frac{m_f}{m_a} \quad (2)$$

where the m_f (gram) is the mass of adsorbed oil on adsorbents, and m_o (gram) is the mass of initial oil in solution (gram). The m_a corresponds to the mass of adsorbents before adsorption in grams. The obtained data was modeled using Freundlich and Langmuir isotherm based on linearization equations (3) and (4) [23,24].

$$\ln C_e = \frac{1}{n} \ln C_e + \ln K_f \quad (3)$$

$$\frac{C_e}{q_e} = \frac{C_e}{q_m} + \frac{1}{K_L q_m} \quad (4)$$

where C_e (mg.L^{-1}) is the final concentration at equilibrium. The adsorbent absorbs the amount of solute at equilibrium, which is described as q_e (mg.g^{-1}). K_f and $\frac{1}{n}$ are Freundlich parameters that represent adsorption capacity and adsorption intensity. The Langmuir constant of q_m is adsorption capacity, and K_L reflects adsorption affinity energy. The separation factor (R_L) is calculated based on equation (5) [24]. C_o (mg.L^{-1}) is the solute initial concentration. The isotherm parameters were determined and calculated using slope and intercept of isotherm plotting

$$R_L = \frac{1}{1 + K_L C_o} \quad (5)$$

Kinetic adsorption of the pseudo-first-order and the pseudo-second-order was determined by equations (6) and (7), respectively [25].

$$\ln (q_e - q_t) = \ln q_e - k_1 t \quad (6)$$

$$\frac{t}{q_t} = \frac{t}{q_e} + \frac{1}{k_2 q_e^2} \quad (7)$$

where the constant of q_t represents the amount of adsorbate per adsorbent in t (minute) time. The amount of adsorbed adsorbate per gram of adsorbents in equilibrium is symbolled as q_e (mg.g^{-1}). The parameters of k_1 and k_2 show the pseudo-first-order and pseudo-second-order constant rates. The pseudo-first-order graph was plotted in time (minutes) versus ln $(q_e - q_t)$. The correlation between time (minutes) and $\frac{t}{q_t}$ was drawn to describe adsorption in the pseudo-second-order.

3. RESULTS AND DISCUSSION
3.1. Adsorbent Characteristics

Figure 1 shows the surface morphology of the adsorbent from the tamarind fruit shell before and after activation with chemical agents. Adsorbent without chemical activation had a solid structure and a small pore. Chemical activation created the honeycomb formation, the porous structure, and the gap between pores becoming small.
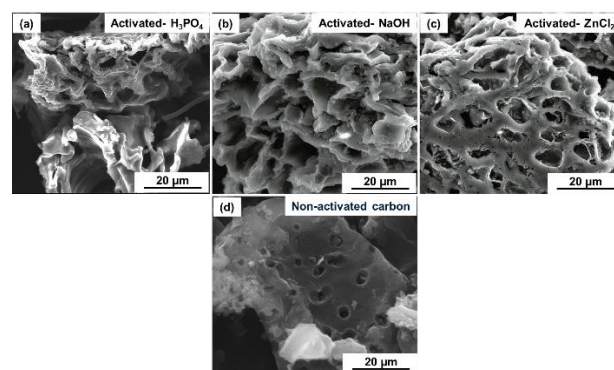

Figure 1. Morphology of adsorbents from tamarind fruit shell with activation (a) using H$_3$PO$_4$; (b) using NaOH; (c) using ZnCl$_2$; and (d) without chemical activation.

The morphology surface of the activated carbon, likely resulting from the chemical activation process using H$_3$PO$_4$, NaOH, and ZnCl$_2$, was shown in Figure 1 (a-c). Figure 1 (a and b) shows that H$_3$PO$_4$ and NaOH-activated carbon had a larger pore size and a thicker pore channel compared with ZnCl$_2$-activated carbon. The activation of carbon using H$_3$PO$_4$ and NaOH promoted the formation of a porous structure, leading to pore development. These large pores contributed to an increased surface area, as previously reported. The results are

consistent with findings from earlier studies [26,27]. The generation of more porous structures is caused by the diffusion of H_3PO_4 and NaOH into the organic material, which leads to the basic and acid-carbon reaction [28]. The formation of phosphate and polyphosphate stimulates the dilation process that develops pore structure after acid elimination [29]. Moreover, the solid structure was formed because the phosphate ester layer can avoid excessive burn-off during activation [30]. While, uneven pore structure formation of $ZnCl_2$ activated carbon as shown in Figure 1 (c) is contributed by corrosive hydroxy dichlorozinc acid, a salt and water reaction product [31].

Table 1 depicts the oil adsorption capacity of activated carbon synthesized using three different chemical activating agents: phosphoric acid (AC-H_3PO_4), sodium hydroxide (AC-NaOH), and zinc chloride (AC-$ZnCl_2$). For each sample, the adsorption process was observed at intervals of 10, 20, 30, 40, 50, and 60 minutes. The clarity of the oil-contaminated water gradually increases over time for all activators, indicating progressive oil removal. Among the three, AC-H_3PO_4 shows rapid adsorption with a clear solution achieved by 30 to 40 minutes, suggesting high adsorption efficiency. AC-NaOH exhibits slower oil removal, with significant turbidity still observed up to 30 minutes, although clarity is achieved by 60 minutes. AC-$ZnCl_2$ shows intermediate performance with oil visibly reduced by 30 minutes and nearly complete removal by 50 to 60 minutes. This visual evidence supports the comparative effectiveness of activation agents in producing porous activated carbon suitable for oil adsorption, with phosphoric acid-treated carbon performing most efficiently under the tested conditions.

Table 1. Photographic comparison of oil adsorption performance using activated carbon (AC) prepared with different chemical activating agents (H_3PO_4, NaOH, $ZnCl_2$) over varying contact times (10 to 60 minutes).

Initially, oily wastewater had a distinctly black colour due to the presence of the used lubricant. Even after treatment, the treated oily wastewater using NaOH-activated carbon still retained a black colour, indicating that the significant oil content remained in the solution. Nevertheless, wastewater after treatment using H_3PO_4 and $ZnCl_2$-activated carbon exhibits a much clearer solution than treatment using NaOH, even only after 10 minutes of treatment. The clearness level between the solution after treatment using H_3PO_4 and $ZnCl_2$-activated carbon was not easily distinguishable. However, the oil removal efficiency data show that the treated solution with H_3PO_4 achieved the highest removal efficiency.
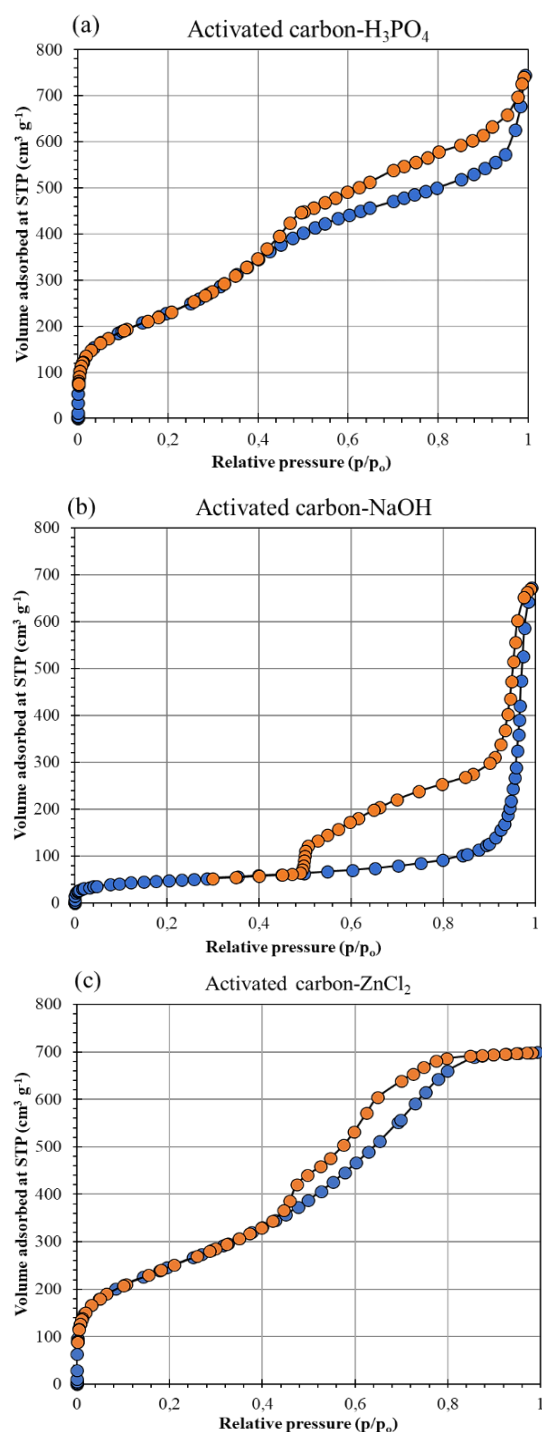
Figure 2. N_2 sorption isotherm of activated carbon (AC) prepared using different activation agent: (a) H_3PO_4, (b) NaOH and (c) $ZnCl_2$.

Figure 2 (a–c) illustrates that the adsorption–desorption isotherms of the activated carbon align with a Type IV isotherm, as classified by the International Union of Pure and Applied Chemistry (IUPAC). A key characteristic of Type IV isotherms is the presence of a hysteresis loop, which results from capillary condensation within mesopores and leads to limited adsorption at higher relative pressures. The pore size distribution, ranging from 2 to 20 nm as shown in Figure 2 (a–c), confirms the mesoporous structure of the material. BET analysis data such as pore size, specific surface area, and pore volume are presented in Table 2. From BET results confirmed that the SEM analysis image, and that the tamarind shell H_3PO_4-activated carbon had a larger pore size and higher specific surface area. Using H_3PO_4, NaOH and $ZnCl_2$, activated carbons had pore sizes of 37.14; 31.43; and 29.27 nm, respectively. The increase in pore size led to an increase in the specific surface area (SSA) of adsorbents. SEM analysis confirms the development of carbon pores following activation with three different agents (i.e., H_3PO_4, NaOH, and $ZnCl_2$). The N_2 adsorption at low relative pressures suggests the presence of predominantly microporous structures. The spesific surface area of activated carbon using H_3PO_4, NaOH and $ZnCl_2$ determined by the BET method is 617.59 $m^2.g^{-1}$ and 422.41 $m^2.g^{-1}$, 576.33 $m^2.g^{-1}$, respectively. The results showed that the activated carbon with H_3PO_4 activator has the specific surface area larger than other activation agent both NaOH and $ZnCl_2$.

Table 2. BET analysis data of activated carbon using H_3PO_4, NaOH and $ZnCl_2$ as activator agents.

Activator	H_3PO_4	NaOH	$ZnCl_2$
Average pore diameter (nm)	37.14	31.43	29.27
Specific surface area (m^2 gram^{-1})	617.59	422.41	576.33
Pore volume (ml gram^{-1})	0.812	0.755	0.716

3.2. Effect of Activating Agents on Surface Functional Groups of Activated Carbon: FTIR Analysis

The FTIR spectra of the activated carbon samples synthesized using H_3PO_4, NaOH, and $ZnCl_2$ as activating agents are presented in Figure 3. These spectra provide insight into the types and intensities of surface functional groups present, which directly influence adsorption performance, particularly for polar or complex molecules such as oil lubricants. The spectrum of H_3PO_4-activated carbon exhibits prominent absorption peaks around ~3400 cm^{-1}, corresponding to the O–H stretching vibrations of hydroxyl groups, indicating the presence of abundant surface –OH groups, which enhance hydrophilicity and potential hydrogen bonding interactions [32]. A notable peak near ~1700 cm^{-1} is attributed to C=O stretching of carboxylic or lactonic groups. Additionally, broad bands in the region 1000–1250 cm^{-1} correspond to P=O and P–O–C stretching vibrations, confirming the incorporation of phosphate functionalities derived from H_3PO_4. These oxygenated and phosphorus-containing groups can improve the adsorption capacity for polar compounds through electrostatic interactions and hydrogen bonding. In contrast, the NaOH-activated carbon spectrum shows less intense O–H stretching bands, and relatively more defined peaks in the ~1570 to 1600 cm^{-1} region, which are typically assigned to C=C skeletal vibrations of aromatic rings. This suggests a more graphitized carbon structure with fewer oxygenated groups, consistent with the strong basicity of NaOH promoting the removal of surface oxygen functionalities during activation [33]. However, the presence of residual –OH and C=O groups still supports a moderate degree of polarity. The $ZnCl_2$-activated carbon displays strong and broad peaks at ~3400 cm^{-1}, indicating the presence of O–H groups, similar to H_3PO_4-treated carbon. Peaks at ~1620 cm^{-1} correspond to aromatic C=C and C=O stretching, while absorption in the 1000–1200 cm^{-1} region suggests the presence of C–O bonds, often associated with phenolic or

ether groups. $ZnCl_2$ acts as a dehydrating agent during activation, promoting the formation of porous carbon and retaining oxygen functionalities [34]. Overall, the FTIR spectra confirm that H_3PO_4 activation introduces the most diverse and intense polar functional groups, which can enhance oil adsorption via chemical interactions, while NaOH yields a more hydrophobic surface, and $ZnCl_2$ provides a balance between porosity and functional group retention.
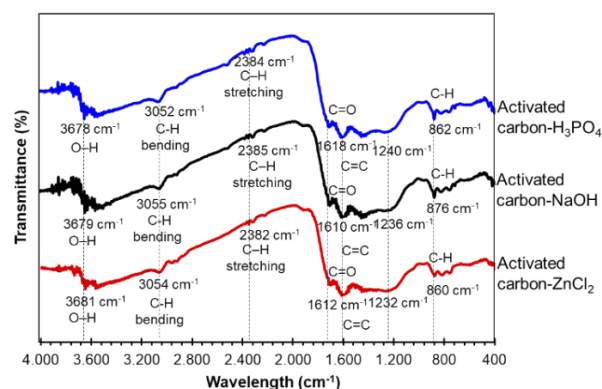

Figure 3. FTIR spectra of tamarind fruit shell activated carbon with activation using NaOH, $ZnCl_2$, and H_3PO_4.

The X-ray diffraction (XRD) patterns shown in Figure 4 reveal differences in the crystallinity characteristics of adsorbents derived from tamarind shell activated with NaOH, $ZnCl_2$, and H_3PO_4. The broad diffraction peak centered at approximately $2\theta \approx 22$–24°, commonly indexed to the (002) plane of graphite-like carbon, indicates the presence of amorphous carbon domains with short-range order. This broad peak indicates the amorphous or partially ordered nature of the carbon structure, which is common in chemically activated carbons [32]. The low intensity of peak and broad width confirm a lack of long-range crystalline order. Unlike $ZnCl_2$ or NaOH-activated carbons, H_3PO_4 activation tends not to introduce significant crystalline inorganic residues, provided proper post-washing is performed. However, in some cases, minor and broad features in the $2\theta = 26$°–34° range may appear, which could be attributed to phosphate residues or metal phosphate complexes (e.g., C–O–P or

C–P=O bonds), especially if the washing was insufficient [35]. These phosphate-containing groups can play a beneficial role in enhancing surface polarity and functional group density. The absence of sharp, crystalline peaks in H_3PO_4-activated carbon as opposed to $ZnCl_2$-activated samples confirms that this activation method primarily contributes to pore development and functional group incorporation without significantly crystallizing the carbon or forming residual mineral phases [33]. For the NaOH-activated carbon, a sharp but low-intensity peak is observed near $2\theta \approx 43.8°$, corresponding to the (100) plane, further confirming partial graphitization of the carbon matrix. However, compared to $ZnCl_2$-activated carbon, this sample presents a broader and more diffuse pattern, signifying a higher degree of amorphous character due to aggressive alkali activation, which etches the carbon framework and introduces porosity [33]. Unlike the others, the $ZnCl_2$-activated carbon exhibits several distinct sharp diffraction peaks overlaid on the broad (002) carbon peak. These sharper peaks are indicative of residual inorganic crystalline phases (e.g., ZnO or Zn species), often retained even after washing, especially at high $ZnCl_2$ concentrations or incomplete post-treatment. The presence of these crystalline impurities contributes to the intensity and sharpness of the diffractogram at $2\theta \approx 31.7°$, $34.4°$, and $36.2°$, which can be indexed to ZnO reflections (JCPDS card no. 36-1451) [34].
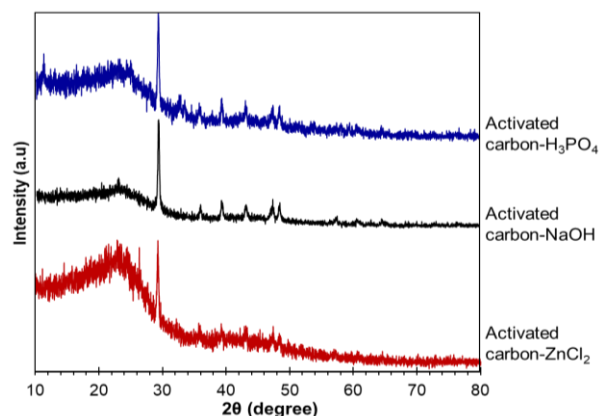

Figure 4. X-ray diffraction patten of activated carbon from tamarind shell with activation using H_3PO_4, NaOH, and $ZnCl_2$.

3.3. Effect of Initial Concentration

The influence of initial oil concentration on adsorption performance is presented in Figure 5. Figure 5 (a) shows that the oil removal efficiency decreased from 50-90% to around 30-40% as the initial concentration increased from 5,000 to 15,000 $mg.L^{-1}$. The increase in initial oil concentration resulted in a decrease in the oil removal efficiency but increased the oil adsorption capacity, as presented in Figure 5 (b). The adsorption capacity experienced a significant increase by approximately 0.4 $mg.g^{-1}$ in initial oil concentrations between 5,000 and 15,000 $mg.L^{-1}$. The previous study presented a similar result, in which initial concentration increases adsorption oil capacity and decreases the remaining active site [36]. This finding demonstrates that the initial concentration is the primary driving force for overcoming mass transfer restriction between the adsorbate and adsorbent [37,38]. The adsorbent with phosphorus acid activator had the highest removal efficiency among different activated carbons because of the larger surface area and pore sizes.
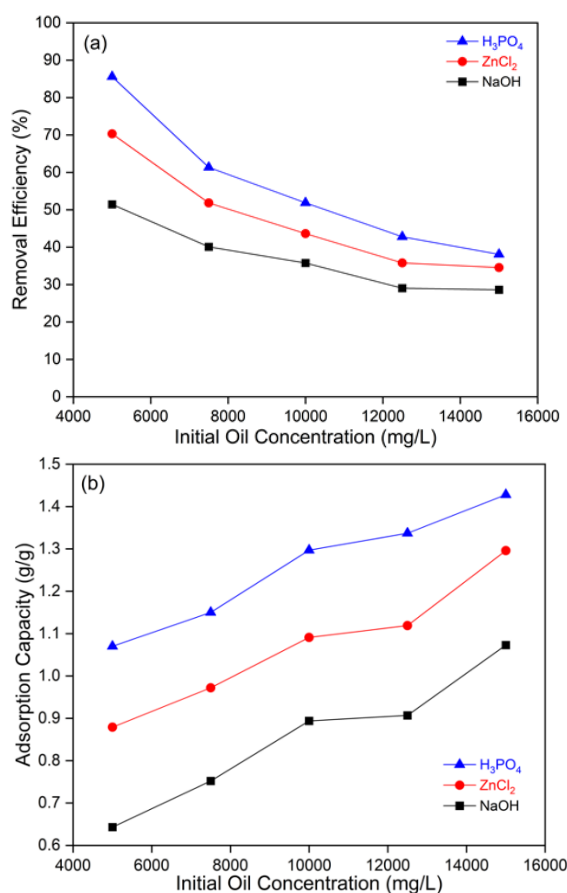
Figure 6. Effect of contact time on oil removal efficiency.

Figure 5. Effect of initial oil concentration on oil (a) removal efficiency, and (b) adsorption capacity.

3.4. Effect of Contact Time

Contact time affects not only the interaction between the surface and the contaminant but also the adsorption rate. Figure 6 presents a correlation between adsorption contact time and oil removal efficiency. The graph shows that the oil removal efficiency increased with contact time. The high curve slope at the beginning demonstrated that oil uptake rates were rapid until reaching a contact time of 10 minutes, with removal efficiencies around 40 to 70%. Many vacant active sites and a weakening attractive force between adsorbate and adsorbent support the initial faster adsorption rate [39].
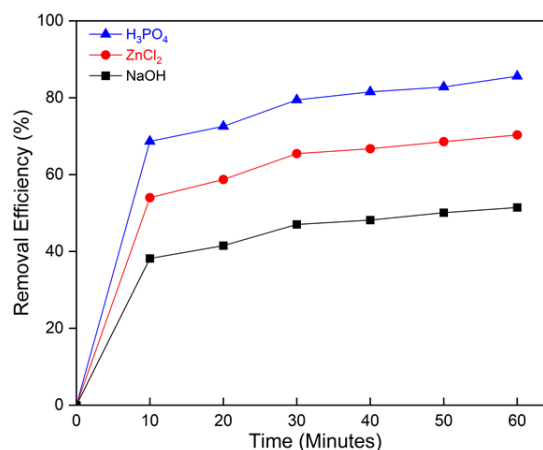
The adsorption rate was slowed down after equilibrium. It was proven that increasing contact time did not increase oil adsorption significantly. After saturation, the empty site cannot be occupied because of the repulsive force between the solute particle, solid, and bulk phase [40]. The adsorbent with H_3PO_4 activator had twice the oil removal efficiency of the NaOH activator. The H_3PO_4-activated carbon reached above 80% removal efficiency at 60 minutes of contact time. However, the adsorption with $ZnCl_2$ and NaOH activation shows that the prolonged contact time until 60 minutes had less than 70% oil removal efficiencies. H_3PO_4-activated carbon had the highest performance because of its higher surface area, pore diameter, and high pore volume than $ZnCl_2$-activated carbon, as previously explained.

3.5. Effect of Adsorbent Dose

Figure 7 presents the impact of the adsorbent dose on oil adsorption. The increase in adsorbent dose resulted in higher oil removal efficiency. The doses of activated carbon (AC) using H_3PO_4 and $ZnCl_2$ ranged from 0.5 to 1.5 grams, leading to a significant rise in oil removal from above 20% to 80%. However, the adsorbent with alkali activation showed the lowest removal efficiency among three different adsorbents. For adsorbents with NaOH activators, oil removal efficiency increased from below 20% to just around 70% with the same dose range.
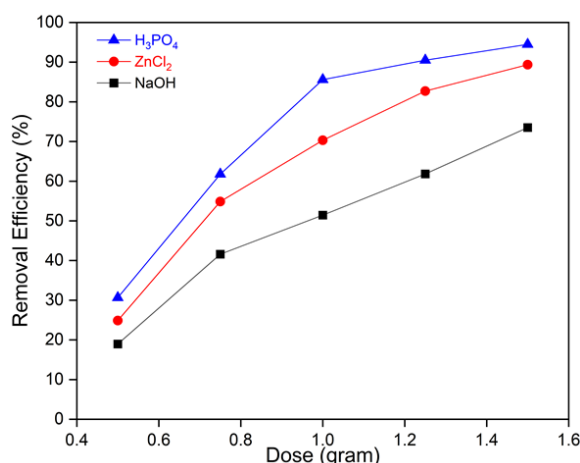
Figure 7. Effect of dose on oil removal efficiency.

Figure 8. Effect of temperature on oil removal efficiency.

H_3PO_4-activated carbon had a high oil uptake rate at the dose of 0.5 to 1.0 gram, but the increased dose of 1.5 gram only increased oil removal efficiency slightly until reaching equilibrium. Increasing adsorbent doses provide a higher active binding site. Thus, it increases the pollutant update rate on the surface of the adsorbent. More available active sites caused a higher chance of solute-adsorbent interaction [41,42].

3.6. Effect of Temperature
Figure 8 illustrates the effect of varying temperatures of 30 to 70°C on oil removal efficiency. The result revealed that the removal efficiency increased gradually between temperatures 30 to 60°C. After a temperature of 60°C, the removal efficiency for all types of activated carbon decreased slightly by around 2%. This finding indicated that oil adsorption on tamarind adsorbent is an endothermic process [43]. The low viscosity of the solution at low temperatures has led to crowded pore conditions that lower adsorbate uptake [44]. In contrast, the decreased viscosity at high temperatures causes pores to be easily penetrated, leading to increased adsorption [45,46]. Furthermore, the high oil uptake at higher temperatures is correlated with weak hydrogen bonds and van der walls force, which create a high strength of physical interaction between the oil molecule and the surface of the adsorbent [39].
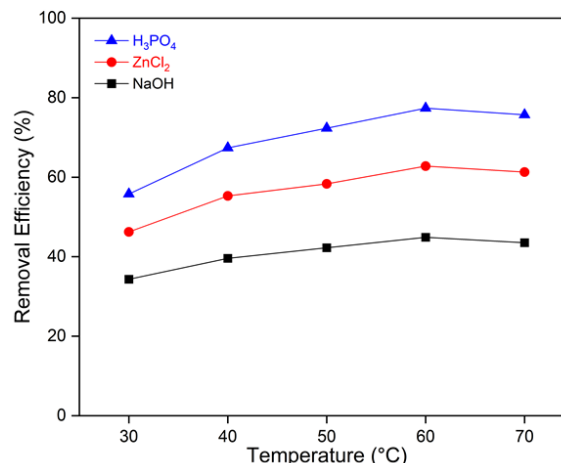
3.7. Effect of pH
The initial pH of oil wastewater affected oil adsorption because pH influences the surface charge of activated carbon and ionization of the solution [47]. The pH of the solution determines alterations in surface characteristics, binding sites, and oil emulsion breakdown [48]. The study of pH influence on oil adsorption is presented in Figure 9. Increasing the initial pH from 4 to 7 increased oil removal efficiency. The removal efficiency decreased gradually at an initial pH above 7. With a phosphorus acid activator, the adsorbent has an oil removal efficiency of 68.96% at a pH of 4, which increased gradually and reached a peak of 85.6% at a pH of 7. Increasing the initial pH decreased the oil removal efficiency considerably to 66.08 % at a pH of 10. The competition between hydroxide ions and oil molecules in the solution in strongly acidic conditions decreases oil removal efficiency [49,50]. The adsorbent surface had a negative charge at alkali pH because of the abundance of hydroxyl functional groups in the solution. The negative charge of the solution affected electrostatic repulsion, which decreased the degree of oil de-emulsification [51,52].
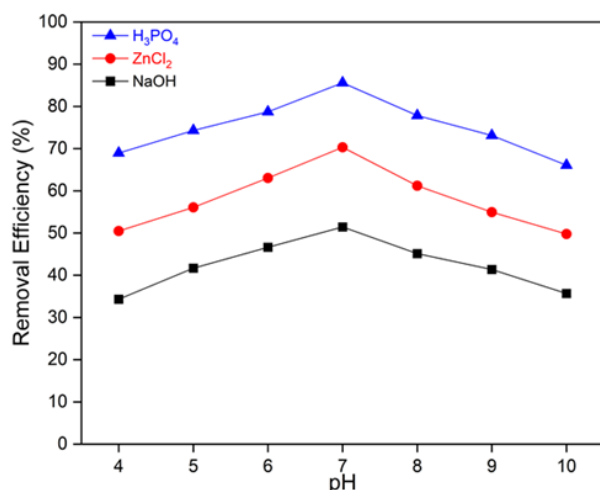
Figure 9. Effect of pH on oil removal efficiency.

3.8. Isotherm Studies

Adsorption isotherm describes the interaction of solute on the surface of the adsorbent in equilibrium conditions. The adsorption experiment data was mathematically modelled using the Freundlich and Langmuir isotherm. Isotherm studies were conducted in 250 mL of 5000 mg.L^{-1} synthesis oil wastewater that was mixed with 800 rpm for 10 to 60 minutes. Figure 10 showed the plotting of Freundlich and Langmuir isotherm.The isotherm parameter obtained from the intercept and slope of plotting data is shown in Table 3. For activated carbon using H$_3$PO$_4$ and ZnCl$_2$, the Langmuir isotherm had a higher coefficient correlation ($R^2 > 0.9950$) than the Freundlich isotherms. Adsorption using tamarind carbon activated using NaOH also has an approximate coefficient correlation ($R^2 > 0.9945$) to 1. Thus, the adsorption was best fitted with Langmuir isotherm. Past research findings also demonstrate that oil adsorption using biomass followed the Langmuir isotherm [53–55].
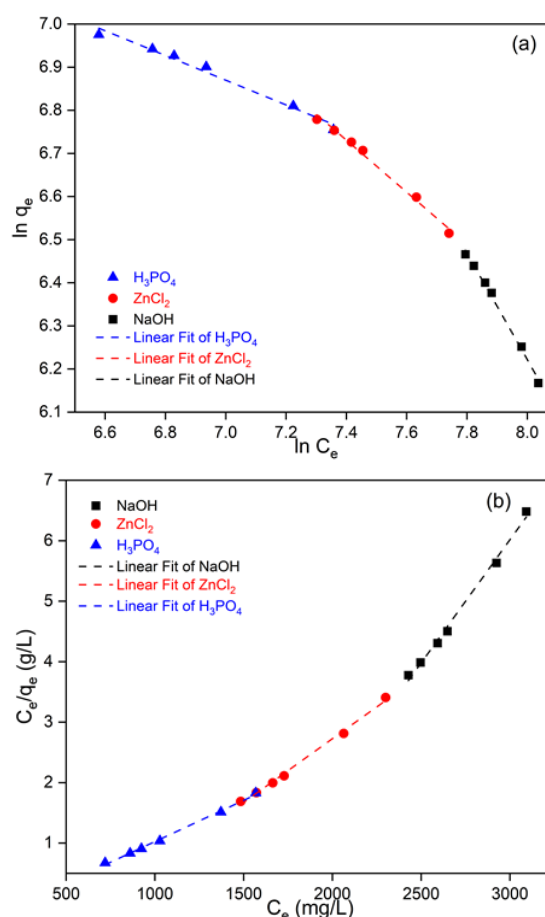

Figure 10. Plotting of (a) Freundlich and (b) Langmuir Isotherm.

The Langmuir isotherm indicates that adsorbate is adsorbed on the monolayer surface in adsorbate [56]. The adsorbent has a uniform energy binding site, so it forms the one adsorption layer. The single binding site only adsorbed one solute and can no longer occupy adsorbate, so there is no competition between adsorbate and adsorbent [13,24]. Based on isotherm calculation, the adsorbent carbon that was activated by phosphorus acid had the highest adsorption capacity of 714.286 mg.h^{-1}. The Langmuir isotherm has R$_L$ values of 0.2939 and 0.0600 for H$_3$PO$_4$ and ZnCl$_2$ activation agents. The R$_L$ value between 0 and less than 1 indicates that the adsorbate is favourable for adsorbents [44]. Parameter (n) of Freundlich supports favourable characteristics between adsorbent and adsorbate. The Freundlich isotherm had n values of $1 < n < 4$ for both activated carbon using H$_3$PO$_4$ and ZnCl$_2$. The Freundlich

constant of 0 < n < 10 exhibits a good affinity between the adsorbate and adsorbents [57].

Table 3. Coefficient of Freundlich and Langmuir adsorption isotherm.

Activator Agent	H_3PO_4	NaOH	$ZnCl_2$
Freundlich Isotherm			
n	3.4892	0.8092	1.6559
$\ln K_f$	8.8759	11.201	16.108
R^2	0.9826	0.9953	0.9921
Langmuir Isotherm			
q_m (mg g^{-1})	714.29	342.92	476.19
K_L (10^{-3})	0.48	31.32	25.41
R_L	0.2939	0.0078	0.0601
R^2	0.9969	0.9945	0.9957

3.9. Kinetics Studies

Adsorption kinetic describes the solute transfer rate on the surface of adsorbents and the mechanism of adsorption. The kinetics study was conducted in contact time of 10 to 60 minutes, with an oil initial concentration of 5,000 mg.L^{-1} with an adsorbent dosage of 1 gram, then mixed using a rate of 800 rpm. Figure 11 shows the graph from plotting experimental data using pseudo-first-order and pseudo-second-order kinetics. Coefficient correlation (R^2) shows the linearity between the axis and ordinal. The plot of pseudo-second-order kinetics has a high coefficient correlation of 0.99 for all chemical agents activated carbon. However, the plot of the pseudo-second-order has a lower coefficient correlation ($R^2 < 0.97$). The higher R^2 shows that the adsorption of oil using activated carbon from tamarind fruit shells follows the pseudo-second-order. The result of the pseudo-second-order kinetics was also reported in the previous studies [58,59]. The pseudo-second-order assumes that the adsorption mechanism is chemisorption [25,60]. The square number of the vacant active site in the adsorbent surface is equal to the binding rate in pseudo-second-order kinetics.
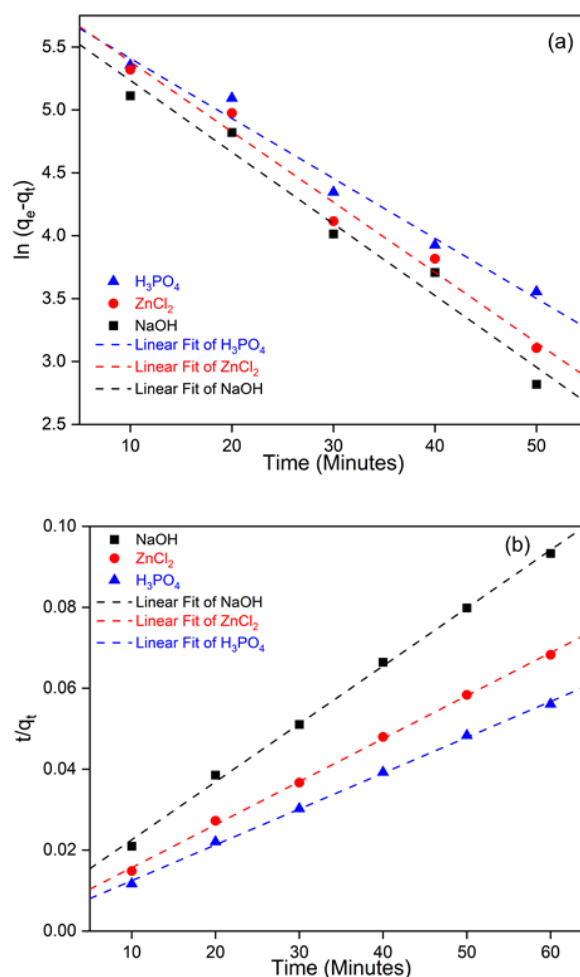

Figure 11. Plotting of (a) Pseudo-First-Order (PFO), and (b) Pseudo-Second-Order (PSO).

The slope and intercept of the kinetic plot were used to determine the kinetics coefficients. The rate constants of k_1 and k_2 were calculated based on the slope and intercept values. Table 4 shows the pseudo-first-order and pseudo-second-order coefficients. The adsorption capacity of pseudo-second-order had a close value with experimental adsorption capacity, so the pseudo-second-order kinetics was more appropriate to describe oil adsorption on tamarind activated carbon.

Table 4. Kinetics coefficient of pseudo-first-order and pseudo-second-order.

Activator Agent	H₃PO₄	ZnCl₂	NaOH
Q_e exp (mg.g⁻¹)	1070	879	643
Pseudo First Order			
Q_e (mg.g⁻¹)	360.14	380.62	331.92
K_1 (10^3 min⁻¹)	47.7	55.8	57.0
R^2	0.9801	0.9800	0.9709
Pseudo Second Order			
Q_e (mg g⁻¹)	1119.11	909.091	714.28
K_2 (10^{-5} min⁻¹)	23.61	24.20	22.50
R^2	0.9986	0.9989	0.9981

3.10. Interaction Mechanism Between Lubricating Oil and Activated Carbon Activated with ZnCl₂, NaOH, and H₃PO₄

The adsorption of lubricating oil onto activated carbon (AC) derived from various chemical activating agents (ZnCl₂, NaOH, and H₃PO₄) was found to follow pseudo-second-order kinetics, suggesting that the rate-limiting step involves chemisorption, where adsorbate molecules form chemical bonds with surface functional groups on the adsorbent [32]. This kinetic behavior indicates that the interaction is not governed purely by surface area or physical attraction but is significantly influenced by chemical affinity and surface functionality introduced during activation. ZnCl₂ activation promotes extensive dehydration, aromatization, and crosslinking of the biomass precursor, leading to high porosity and a large surface area. FTIR and XRD results also suggest the presence of phenolic –OH, ether (C–O–C), and residual Zn-containing species on the surface [35]. Chemical interactions: The surface –OH and ether groups can interact with polar components or additive molecules in the lubricating oil via hydrogen bonding and Lewis acid–base interactions. Residual Zn²⁺ species may also act as coordination centers, attracting polar ester or hydroxyl compounds within the oil matrix. These interactions enhance the chemical affinity between the carbon surface and polar oil components, supporting the pseudo-second-

order kinetic behavior. In the case of NaOH activation leads to a highly microporous structure and partial removal of surface oxygen groups, producing a more aromatic or graphitized surface with fewer acidic sites [33]. While the hydrophobic surface is suited for van der Waals interactions with non-polar hydrocarbons in the oil, the presence of some residual –OH or carbonyl groups allows for π–π interactions and dipole-induced dipole forces. The pseudo-second-order fit implies that although the surface is less polar, the functional groups that remain (e.g., carboxylic and phenolic) still engage in chemical interactions, likely with polar additives or degradation products in the oil. Meanwhile, Phosphoric acid (H₃PO₄) activation introduces a high density of oxygenated (–OH, –COOH, C=O) and phosphorus-containing functional groups (P–O–C, P=O) [34]. This produces a strongly polar and acidic surface. These functional groups facilitate chemisorption via hydrogen bonding, electrostatic attraction, and even esterification reactions with polar compounds in the lubricating oil. Particularly, the P–O–H and C=O groups act as active binding sites for adsorption of oxygenated oil components or degradation products (e.g., oxidized hydrocarbons, esters) [59]. This rich chemistry contributes to the highest affinity for oil adsorption, often reflected in higher adsorption capacity and faster kinetics for both well explained by the pseudo-second-order model.

4. CONCLUSIONS

The research investigation found that tamarind fruit shell-derived activated carbon was a potential adsorbent to remove oil concentrations in wastewater. Chemical activation successfully enhances the pore morphology formation, pore sizes, and specific surface area in adsorbents, as proven by SEM and BET analysis. The specific surface area (BET) of activated carbon prepared using different chemical activators (H₃PO₄, NaOH, and ZnCl₂) shows a clear variation depending on the activating agent used: H₃PO₄-activated carbon exhibits the

highest specific surface area of 617.59 $m^2.g^{-1}$, indicating superior porosity development and effective activation. $ZnCl_2$-activated carbon follows with a specific surface area of 576.33 $m^2.g^{-1}$, which is also relatively high, suggesting good textural properties. NaOH-activated carbon has the lowest specific surface area at 422.41 $m^2.g^{-1}$, implying comparatively lower pore development. The results indicate that H_3PO_4 is the most effective activating agent among the three, producing activated carbon with the highest BET surface area. This suggests that H_3PO_4 promotes more extensive pore formation and a greater accessible surface area, which is beneficial for adsorption applications. $ZnCl_2$ also performs well, while NaOH, although effective, results in a significantly lower surface area. These differences can be attributed to the distinct chemical activation mechanisms and interactions between each activating agent and the carbon precursor during the activation process. The equilibrium data was modelled using the isotherm and kinetics equation. The results show that the equilibrium data fitted best with Langmuir isotherm and pseudo-second-order kinetics. The oil adsorption onto tamarind fruit shell-derived activated carbon mechanism is chemisorption. The activated carbon using H_3PO_4 as activation agent has the highest oil adsorption capacity due to the largest pore size, specific area, pore volume and more porous structures.

REFERENCES

[1] M. L. Chan, Frost & Sullivan's 2024 ASEAN Automotive Growth Outlook, https://store.frost.com/frost-sullivan-s-2024-asean-automotive-growth-outlook.html.

[2] ASEAN Automotive Federation (AAF), Asean Automotive Federation 2023 Statistics, https://www.asean-autofed.com/.

[3] D. Susilo, Macro Environment Analysis of Automotive Industry in Indonesia, *BISE: Jurnal Pendidikan Bisnis dan Ekonomi*, vol. 4, no. 2, pp. 150–158, 2018.

[4] J. Guo, C. Wang, Analysis of Contaminants in Vehicle Maintenance and Repair Enterprise, *Advances in Engineering Research*, vol. 159, pp. 228–232, 2018.

[5] P. Singh, V. Kadam, Y. Patil, Isolation and development of a microbial consortium for the treatment of automobile service station wastewater, *J. Appl. Microbiol*, vol. 132, no. 2, pp. 1048–1061, 2022.

[6] M. Bujang, N. A. Ibrahim, A. Eh Rak, Physicochemical quality of oily wastewater from automotive workshop in Kota Bharu, Kelantan Malaysia, *Aust. J. Basic Appl. Sci.*, vol. 6, no. 9, pp. 748–752, 2012.

[7] H. S. Abd El-Gawad, Oil and Grease Removal from Industrial Wastewater Using New Utility Approach, *Advances in Environmental Chemistry*, vol. 2014, p. 16878, 2014.

[8] S. Putatunda, S. Bhattacharya, D. Sen, C. Bhattacharjee, A review on the application of different treatment processes for emulsified oily wastewater, *Int. J. Environ. Sci. Technol.*, vol. 16, pp. 2525–2536, 2019.

[9] A. Bhattacharyya, L. Liu, K. Lee, J. Miao, Review of Biological Processes in a Membrane Bioreactor (MBR): Effects of Wastewater Characteristics and Operational Parameters on Biodegradation Efficiency When

Treating Industrial Oily Wastewater, *J. Mar. Sci. Eng.,* vol. 10, no. 9, p. 1229, 2022.

[10] H. J. Tanudjaja, C. A. Hejase, V. V. Tarabara, A. G. Fane, J. W. Chew, Membrane-based separation for oily wastewater: A practical perspective, *Water Research*, vol. 156, pp. 347–365, 2019.

[11] Y. Sun, H. Li, G. Li, B. Gao, Q. Yue, X. Li, Characterization and coagulation behavior of polymeric aluminum ferric silicate for high-concentration oily wastewater treatment, *Chem. Eng. Res. Des.*, vol. 119, pp. 23–32, 2017.

[12] M. A. H. Aswadi, M. A. Shukor, M. A. Ishak, Kinetics and Effects of Process Parameters on Oil Adsorption using Activated Carbon from Rubber Seed Kernels (Hevea brasiliensis), *Chem. Eng. Trans.*, vol. 106, pp. 991–996, 2023.

[13] H. J. Al-Jaaf, N. S. Ali, S. M. Alardhi, T. M. Albayati, Implementing eggplant peels as an efficient bio-adsorbent for treatment of oily domestic wastewater, *Desalination Water Treat*, vol. 245, pp. 91–100, 2022.

[14] S. Martini, S. Afroze, K. A. Roni, Modified eucalyptus bark as a sorbent for simultaneous removal of COD, oil, and Cr(III) from industrial wastewater, *Alexandria Engineering Journal*, vol. 59, no. 3, pp. 1857–1867, 2020.

[15] N. S. M. Thani, R. M. Ghazi, N. Ismail, Response Surface Methodology Optimization of Oil Removal Using Banana Peel as Bisorbent, *Malaysian Journal of Analytical Science*, vol. 21, no. 5, pp. 1125–1134, 2017. doi: 10.17576/mjas-2017-2105-12.

[16] D. Peng, S. Cheng, H. Li, X. Guo, Effective multi-functional biosorbent derived from corn stalk pith for dyes and oils removal, *Chemosphere*, vol. 272, p. 129963, 2021.

[17] J. S. Vaza, S. A. Bhalerao, Biosorption of Zinc (II) from Aqueous Solution using Tartaric Acid Modified Tamarind (*Tamarindus indica* L.) Pod Shell Powder, *Int. J. Res. Appl. Sci. Eng. Technol.*, vol. 7, no. 1, pp. 500–514, 2019.

[18] S. L. Pandharipande, R. P. Kalnake, Tamarind Fruit Shell Adsorbent Synthesis, Characterization and Adsorption Studies for Removal of Cr(VI) & Ni(II) Ions from Aqueous Solution, *Int. J. Eng. Sci. Emerg. Technol.*, vol. 4, no. 2, pp: 83–89, 2013.

[19] P. G. Radhakrishnan, S. P. Varghese, B. C Das, Application of ethylenediamine hydroxypropyl tamarind fruit shell as adsorbent to remove Eriochrome black T from aqueous solutions – Kinetic and equilibrium studies, *Separation Science and Technology (Philadelphia)*, vol. 53, no. 3, pp. 417–438, 2018.

[20] V. Sivasankar, S. Rajkumar, S. Murugesh, A. Darchen, Tamarind (*Tamarindus indica*) fruit shell carbon: A calcium-rich promising adsorbent for fluoride removal from groundwater, *J. Hazard. Mater.*, vol. 225–226, pp. 164–172, 2012.

[21] Y. Sun, H. Li, G. Li, B. Gao, Q. Yue, X. Li, Characterization and ciprofloxacin adsorption properties of activated carbons prepared from biomass wastes by H_3PO_4 activation, *Bioresour. Technol.*, vol. 217, pp. 239–244, 2016.

[22] A. Toprak, T. Kopac, Carbon Dioxide Adsorption Using High Surface Area Activated Carbons from Local Coals Modified by KOH, NaOH and $ZnCl_2$ Agents, *Int. J. Chem. React. Eng.*, vol. 15, no. 3, p. 20160042, 2017.

[23] J. Bayuo, K. B. Pelig-ba, M. A. Abukari, Isotherm Modeling of Lead (II) Adsorption from Aqueous Solution Using Groundnut Shell as a Low-Cost Adsorbent, *IOSR Journal of*

Applied Chemistry, vol. 11, no. 11, pp. 18–23, 2018.

[24] J. O. Nwadiogbu, V. I. E. Ajiwe, P. A. C. Okoye, Removal of crude oil from aqueous medium by sorption on hydrophobic corncobs: Equilibrium and kinetic studies, *Journal of Taibah University for Science*, vol. 10, no. 1, pp. 56–63, 2016.

[25] E. Piperopoulos, L. Calabrese, E. Mastronardo, S. H. A. Rahim, E. Proverbio, C. Milone, Assessment of sorption kinetics of carbon nanotube-based composite foams for oil recovery application, *J. Appl. Polym. Sci.*, vol. 136, no. 14, p. 47374, 2019.

[26] L. Ernawati, M. Reza, A. C. Synthia, D. A. Kartikasari, I. K. Maharsih, A. Halim, Role of Chemical Activating Agent on the Characteristics of Activated Carbon Derived from Fruit-Peel Waste for Aqueous Dye Removal, *Key Engineering Materials*, vol. 937, pp. 165–180, 2022.

[27] A. Halim, L. Ernawati, M. Ismayati, F. Martak, T. Enomae, Bioinspired cellulose-based membranes in oily wastewater treatment, *Front. Environ. Sci. Eng.*, vol. 16, no. 7, p. 94, 2022.

[28] O. Oginni, K. Singh, G. Oporto, B. Dawson-Andoh, L. McDonald, E. Sabolsky, Effect of one-step and two-step H_3PO_4 activation on activated carbon characteristics, *Bioresour. Technol. Rep.*, vol. 8, p. 100307, 2019.

[29] S. M. Villota, H. Lei, E. Villota, M. Qian, J. Lavarias, V. Taylan, I. Agulto, W. Mateo, M. Valentin, M. Denson, Microwave-Assisted Activation of Waste Cocoa Pod Husk by H_3PO_4 and KOH–Comparative Insight into Textural Properties and Pore Development, *ACS Omega*, vol. 4, no. 4, pp. 7088–7095, 2019.

[30] J. Xu, L. Chen, H. Qu, Y. Jiao, J. Xie, G. Xing, Preparation and characterization of activated carbon from reedy grass leaves by chemical activation with H_3PO_4, *Appl. Surf. Sci.*, vol. 320, pp. 674–680, 2014.

[31] B. Li, J. Hu, H. Xiong, Y. Xiao, Application and Properties of Microporous Carbons Activated by $ZnCl_2$: Adsorption Behavior and Activation Mechanism, *ACS Omega*, vol. 5, no. 16, pp. 9388–9397, 2020.

[32] J. Guo, A. C. Lua, Textural and chemical properties of adsorbent prepared from palm shell by phosphoric acid activation, *Mater. Chem. Phys.*, vol. 80, no. 1, pp. 114–119, 2003.

[33] I. A. W. Tan, A. L. Ahmad, B. H. Hameed, Preparation of activated carbon from coconut husk: Optimization study on removal of 2,4,6-trichlorophenol using response surface methodology, *J. Hazard. Mater.*, vol. 153, no. 1–2, pp. 709–717, 2008.

[34] A. Ahmadpour, D. D. Do, The preparation of activated carbon from macadamia nutshell by chemical activation, *Carbon*, vol. 35, no. 12, pp. 1723–1732, 1997.

[35] P. González-García, Activated carbon from lignocellulosics precursors: A review of the synthesis methods, characterization techniques and applications, *Renew. Sustain. Energy Rev.*, vol. 82, pp. 1393–1414, 2018.

[36] K. Okiel, M. El-Sayed, M. Y. El-Kady, Treatment of oil–water emulsions by adsorption onto activated carbon, bentonite and deposited carbon, *Egyptian Journal of Petroleum*, vol. 20, no. 2, pp. 9–15, 2011.

[37] R. Asadpour, N. B. Sapari, M. H. Isa, K. U. Orji, Enhancing the hydrophobicity of mangrove bark by esterification for oil adsorption, *Water Science and Technology*, vol. 70, no. 7, pp. 1220–1228, 2014.

[38] M. Fathy, M. El-Sayed, M. Ramzi, O. H. Abdelraheem, Adsorption separation of condensate oil from produced water using ACTF prepared of oil palm leaves by batch and fixed bed techniques, *Egyptian Journal of*

Petroleum, vol. 27, no. 3, pp. 319–326, 2018.

[39] U. A. Abel, G. R. Habor, O. I. Oseribho, Adsorption Studies of Oil Spill Clean-up Using Coconut Coir Activated Carbon (CCAC), *American Journal of Chemical Engineering*, vol. 8, no. 2, pp. 36–47, 2020.

[40] S. Saruchi, B. S. Kaith, R. Jindal, V. Kumar, The adsorption of crude oil from an aqueous solution using a *Gum tragacanth* polyacrylic acid based hydrogel, *Pet. Sci. Technol.*, vol. 33, no. 3, pp. 278–286, 2015.

[41] W. Pitakpoolsil, M. Hunsom, Treatment of biodiesel wastewater by adsorption with commercial chitosan flakes: Parameter optimization and process kinetics, *J. Environ. Manage.*, vol. 133, pp. 284–292, 2014.

[42] A. K. Fard, G. Mckay, Y. Manawi, Z. Malaibari, M. A. Hussien, Outstanding adsorption performance of high aspect ratio and super-hydrophobic carbon nanotubes for oil removal, *Chemosphere*, vol. 164, pp. 142–155, 2016.

[43] S. S. Elanchezhiyan, S. M. Prabhu, S. Meenakshi, Effective adsorption of oil droplets from oil-in-water emulsion using metal ions encapsulated biopolymers: Role of metal ions and their mechanism in oil removal, *Int. J. Biol. Macromol.*, vol. 112, pp. 294–305, 2018.

[44] K. AlAmeri, A. Giwa, L. Yousef, A. Alraeesi, H. Taher, Sorption and removal of crude oil spills from seawater using peat-derived biochar: An optimization study, *J. Environ. Manage.*, vol. 250, p. 109465, 2019.

[45] O. Abdelwahab, Assessment of raw luffa as a natural hollow oleophilic fibrous sorbent for oil spill cleanup, *Alexandria Engineering Journal*, vol. 53, no. 1, pp. 213–218, 2014.

[46] S. E. Agarry, K. M. Oghenejoboh, E. O. Oghenejoboh, C. N. Owabor, O. O. Ogunleye, Adsorptive remediation of crude oil contaminated marine water using chemically and thermally modified coconut (Cocos nucifera) husks, *Journal of Environmental Treatment Techniques*, vol. 8, no. 2, pp. 694–707, 2020.

[47] A. Amari, H. S. K. Alawameleh, M. Isam, M. A. J. Maktoof, H. Osman, B. Panneerselvam, M. Thomas, Thermodynamic Investigation and Study of Kinetics and Mass Transfer Mechanisms of Oily Wastewater Adsorption on UIO-66–MnFe$_2$O$_4$ as a Metal–Organic Framework (MOF), *Sustainability*, vol. 15, no. 3, p. 2488, 2023.

[48] R. Wahi, L. A. Chuah, T. S. Y. Choong, Z. Ngaini, M. M. Nourouzi, Oil removal from aqueous state by natural fibrous sorbent: An overview, *Sep. Purif. Technol.*, vol. 113, pp. 51–63, 2013.

[49] T. H. Nazifa, T. Hadibarata, A. Yuniarto, M. S. Elshikh, A. Syafiuddin, Equilibrium, kinetic and thermodynamic analysis petroleum oil adsorption from aqueous solution by magnetic activated carbon, *IOP Conference Series: Materials Science and Engineering*, vol. 495, p. 012060, 2019.

[50] A. El Shahawy, G. Heikal, Organic pollutants removal from oily wastewater using clean technology economically, friendly biosorbent (Phragmites australis), *Ecol. Eng.*, vol. 122, pp. 207–218, 2018.

[51] Y. Li, M. Wang, D. Sun, Y. Li, T. Wu, Effective removal of emulsified oil from oily wastewater using surfactant-modified sepiolite, *Appl. Clay Sci.*, vol. 157, pp. 227–236, 2018.

[52] S. S. D. Elanchezhiyan, S. Meenakshi, Facile Fabrication of Metal Ions-Incorporated Chitosan/β-Cyclodextrin Composites for Effective Removal of Oil from Oily Wastewater, *ChemistrySelect*, vol. 2, no. 35, pp. 11393–11401, 2017.

[53] H. J. Choi, Agricultural bio-waste for adsorptive removal of crude oil in

aqueous solution, *J. Mater. Cycles Waste Manag.*, vol. 21, pp. 356–364, 2019.

[54] M. J. A. Alatabe, H. A. Faris, H. Husham, Natural Biosorbent for Oil Adsorption from Produced Water by Sedge Cane, *J. Ecol. Eng.*, vol. 24, no. 10, pp. 67–76, 2023.

[55] K. G. Akpomie, C. C. Ezeofor, J. U. Ani, S. I. Eze, C. C. Odo, E. A. Onoabedje, Equilibrium isotherms modeling of crude oil sorption from aqua mixture onto *Codiaeum variegatum* stem powder, *Pet. Sci. Technol.*, vol. 37, no. 3, pp. 329–336, 2019.

[56] S. Songsaeng, P. Thamyongkit, S. Poompradub, Natural rubber/reduced-graphene oxide composite materials: Morphological and oil adsorption properties for treatment of oil spills, *J. Adv. Res.*, vol. 20, pp. 79–89, 2019.

[57] K. G. Akpomie, J. Conradie, Treatment of motor oil-contaminated water via sorption onto natural organic lignocellulosic waste: thermodynamics, kinetics, isotherm, recycling, and reuse, *Biomass Convers. Biorefin.*, vol. 13, pp. 10285–10297, 2023.

[58] J.-Q. Hu, S.-Z. Yang, L. Guo, X. Xu, T. Yao, F. Xie, Microscopic investigation on the adsorption of lubrication oil on microplastics, *J. Mol. Liq.*, vol. 227, pp. 351–355, 2017.

[59] N. Lv, X. Wang, S. Peng, H. Zhang, L. Luo, Study of the kinetics and equilibrium of the adsorption of oils onto hydrophobic jute fiber modified via the sol-gel method, *Int. J. Environ. Res. Public Health*, vol. 15, no. 5, p. 969, 2018.

[60] S. Saruchi, V. Kumar, Separation of crude oil from water using chitosan based hydrogel, *Cellulose*, vol. 26, pp. 6229–6239, 2019.